



CHORUS

This is the accepted manuscript made available via CHORUS. The article has been published as:

Homogeneous linewidth broadening and exciton dephasing mechanism in MoTe_2

Sandhaya Koirala, Shinichiro Mouri, Yuhei Miyauchi, and Kazunari Matsuda

Phys. Rev. B **93**, 075411 — Published 4 February 2016

DOI: [10.1103/PhysRevB.93.075411](https://doi.org/10.1103/PhysRevB.93.075411)

Homogeneous linewidth broadening and exciton dephasing mechanism in MoTe₂

Sandhaya Koirala^{*}, Shinichiro Mouri, Yuhei Miyauchi,
and Kazunari Matsuda^{*}

Institute of Advanced Energy, Kyoto University, Uji, Kyoto 611-0011, Japan

ABSTRACT

Spectroscopic studies of mechanically exfoliated monolayer MoTe₂ was performed over a wide temperature range from 4.2 to 300 K. At a low temperature, the photoluminescence (PL) spectra for monolayer MoTe₂ showed two sharp peaks for excitons and charged excitons (trions). The homogeneous linewidth of the exciton peak broadened linearly as the temperature increased. This linear linewidth broadening was caused by acoustic-phonon scattering of the exciton, i.e., shortening of exciton dephasing. The broadening factor due to exciton–acoustic-phonon interactions was found to be 0.11 meV/K. This small value for the exciton–phonon coupling coefficient and the lack of a Stokes shift suggest that exciton-phonon interactions in monolayer MoTe₂ are in the weak coupling regime.

Keywords: Transition metal dichalcogenides, molybdenum ditelluride, infrared emission, spectral broadening, dephasing, exciton, trion

^{*}E-mail address: koirala@iae.kyoto-u.ac.jp, matsuda@iae.kyoto-u.ac.jp

Recently, atomically thin layered transition-metal dichalcogenides (TMDs) in the form MX_2 ($\text{M} = \text{Mo}, \text{W}, \text{X} = \text{S}, \text{Se}, \text{Te}$) have attracted much interest from the viewpoints of their fundamental physics and potential applications^{1,2}. The characteristic optical features of semiconducting two-dimensional (2D) TMDs arise from bound electron-hole pairs (excitons) confined in their atomically thin layers, which play important roles in optoelectronic device applications^{3,4}. Optical studies of TMDs have mainly focused on the model systems MoS_2 , WSe_2 , and MoSe_2 ^{2,5,6}. Newly studied molybdenum ditelluride (MoTe_2) is also TMD that has attracted emerging research interest because of its novel optical properties, including optical gap energy (lowest exciton transition) of 1.09 eV, which is in the near-infrared region^{7,8}. Compared with other Mo-related TMD semiconductors (MoS_2 and MoSe_2), MoTe_2 also has a stronger spin-orbit coupling of 250 meV⁷, which may result in a longer decoherence time for valley and spin degree of freedoms^{9,10} and therefore enable its use in valleytronic devices.

The energy and phase relaxation of excitons influenced by phonon scattering processes is an important issue in the study of low-dimensional semiconductor physics^{11,12}. Indeed, the energy relaxation of excitons in TMDs has been studied by transient absorption and photoluminescence (PL) spectroscopy¹³. However, the mechanism of exciton phase relaxation in TMDs remains unclear because it is difficult to obtain information on exciton dephasing time (or the intrinsic peak linewidths in optical spectra) in well-studied MX_2 TMDs ($\text{M} = \text{Mo}, \text{W}, \text{X} = \text{S}, \text{Se}$)^{4,14}.¹⁵ these monolayer TMDs are unintentionally heavily carrier (electron or hole) doped and thus have relatively complicated optical spectra with overlapping exciton and charged exciton (trion) spectral peaks¹⁶. In contrast, MoTe_2 is a relatively low-

carrier-density semiconductor ¹⁶, which enables the precise determination of its optical spectrum and evaluation of the optical spectral linewidths for excitons.

Herein, we describe the results of spectroscopic analyses of mechanically exfoliated monolayer MoTe₂ from cryogenic temperature 4.2 K to room temperature performed in order to study exciton dephasing and exciton–phonon interactions. At low temperatures, the PL spectra for monolayer MoTe₂ exhibited two sharp excitons (X) and charged exciton (trion X⁻) peaks. The homogeneous linewidth of the exciton peak increased linearly with increasing temperature, suggesting that the exciton dephasing causing the linewidth broadening was dominated by the scattering of excitons by low-energy acoustic phonons. Notably, the obtained linewidth broadening coefficient indicated that the exciton acoustic-phonon interactions in monolayer MoTe₂ are in the weak-coupling regime, which is favorable for applications requiring long exciton coherence times.

MoTe₂ crystals were mechanically exfoliated onto SiO₂/Si and quartz substrates in order to obtain monolayer flakes of MoTe₂. An SiO₂/Si substrate with an SiO₂ thickness of 290 nm was used to clearly identify the atomically thin materials. Atomic force microscopy (AFM) and Raman scattering analyses were conducted to identify the layer thicknesses of the exfoliated MoTe₂ flakes on the substrates. Raman measurements at room temperature was conducted using micro-Raman spectrometer, RAMANtouch (532 nm, 2.33 eV) with a 100× objective (NA = 0.8), the signals were detected in reflection geometry. PL and differential reflectivity measurements from 4.2 to 300 K were conducted using a home-built setup with a 100× objective (NA = 0.5), and the signals were detected using a liq. N₂-cooled InGaAs array. An excitation

wavelength of ~ 550 nm (2.25 eV) with a delivered power of ~ 10 μ W from a super-continuum laser source was used for PL measurements. The white light with very low power ~ 2 μ W from the super-continuum laser source was used for differential reflectivity measurements.

Figure 1 shows Raman scattering spectra for MoTe₂ consisting of different numbers of layers on SiO₂/Si substrates. The optical images of monolayer (ML) and bilayer (BL) MoTe₂ are also shown in the inset on the left side of Fig. 1. The characteristic phonon modes for monolayer MoTe₂ are observed at ~ 172 (A_g^1 mode) and ~ 236 cm^{-1} (E_{2g}^1 mode) in the Raman spectra. The A_g^1 phonon mode is an in-plane vibrational mode that becomes more significant as the layer thickness increases, and the E_{2g}^1 mode is due to the stacking effect of different layers where surface effects are more significant¹⁷. The B_{2g}^1 mode is inactive in the bulk but is allowed for few-layer MoTe₂ due to the breaking of translational symmetry. As expected, for bulk MoTe₂, only two phonon peaks at ~ 174 (A_g^1 mode) and ~ 234 cm^{-1} (E_{2g}^1 mode) are observed, while all three phonon peaks are observed in trilayer and bilayer MoTe₂, and the Raman intensity increases with a decrease in the number of layers (Fig. 1). In contrast, from bilayer to monolayer MoTe₂, the B_{2g}^1 mode disappears and characteristic up and down shifts of the A_g^1 and E_{2g}^1 modes, respectively, are observed in the Raman spectrum, as shown in the inset of Fig. 1. Moreover, a frequency shift of 2 cm^{-1} for the E_{2g}^1 mode is observed, as shown in the inset on the right side of Fig. 1, which is significant proof of the formation of monolayer MoTe₂ and consistent with previously reported result⁷. The formation of monolayer MoTe₂ is also experimentally confirmed determining the height profile of a sample using AFM.

Temperature-dependent PL spectra for monolayer MoTe₂, for which the layer number was confirmed by Raman analysis, as shown in Fig. 1(a), were then obtained from 4.2 to 300 K and are shown in Fig. 2(a). The PL spectrum at 4.2 K has two prominent peaks at 1.19 and 1.17 eV as well a peak due to the Si substrate at 1.10 eV. The two peaks are assigned as emissions from excitons (X) and charged excitons (trions X⁻), respectively^{8,18,19}. The energy separation between the exciton and trion peaks is approximately ~20 meV, which is lower than that in other TMD materials¹⁴. For monolayer MoTe₂ on a quartz substrate, only a PL peak at 1.18 eV attributed to exciton recombination is observed at 4.2 K, (see the Supporting Information, Fig. S1). The relative PL intensity of the exciton and trion peaks varied from flake to flake on the same substrate and on the two different substrates (SiO₂/Si or quartz) because the doped carrier density changes depending on the degree of charge transfer from the substrate to monolayer TMDs²⁰. The observed PL peaks broadens and shifts to lower energies with increasing temperature. The PL spectra were analyzed using spectral fitting procedures in order to evaluate the energy positions and spectral linewidths.

Figures 3(a) and 3(b) show the PL spectra and fitted results (solid black lines) for monolayer MoTe₂ at low temperature 4.2 K and room temperature, respectively. The PL spectra for monolayer MoTe₂ are well reproduced using Voigt functions that takes into account the contributions of homogeneous and inhomogeneous broadening as Lorentzian and Gaussian components, respectively (Figs. 2 and 3). Here, the two PL peaks for the excitons and charged excitons (trions) are mainly considered. Moreover, the PL spectra in the wide temperature range from 4.2 to 300 K are well fitted by these Voigt functions, as shown in Fig. 2.

Figure 4 shows the energy positions of the peaks for the excitons (solid triangles) and trions (blue solid circles) as a function of temperature. Both exciton and trion peaks gradually shift to lower energies with an increase in temperature from 4.2 to 300 K. The spectral energy position of the exciton peak $E_g(0)$ is simulated using the Varshni equation:²¹

$$E_{\text{ex(tr)}}(T) = E_{\text{ex(tr)}}(0) - \frac{\alpha T^2}{T + \beta}, \quad (1)$$

where T is the temperature of the monolayer MoTe₂, α and β are parameters, and $E_{\text{ex(tr)}}(0)$ is the spectral energy position of the excitons (trions) at the zero temperature limit. As shown by the solid lines in Fig. 4, the temperature dependence of the spectral shifts for both excitons and trions in monolayer MoTe₂ is well reproduced using eq. (1). Values for $E_{\text{ex}}(0)$ of 1.19 and 1.17 eV were obtained for the exciton and trion peaks, respectively, and the values for α and β were determined to be 6.4×10^{-4} eV/K and 287 K, respectively. The Varshni equation is known to effectively describe the temperature dependence of band gap shifts in semiconductors. Therefore, the excellent reproduction of the temperature dependence of the exciton (trion) energies using the Varshni equation indicates that the energy of the exciton (trion) peak shift originated from the temperature dependent bandgap shift. It should be noted that we also confirm that the temperature dependence of the exciton (trion) energies is well reproduced using the Vana equation [See supporting information S4].²²

As mentioned above, the PL spectra for monolayer MoTe₂ from 4.2 to 300 K were well reproduced by the fitted results obtained using Voigt functions (solid black lines in Fig. 2). The full width at half maximum (FWHM) of the Lorentzian component,

which corresponds to the homogeneous linewidth, as a function of temperature for the exciton peaks for three different monolayer MoTe₂ two on SiO₂/Si and one on SiO₂ are plotted in Fig. 5. Here, we used that the FWHM of the Gaussian component corresponding to inhomogeneous broadening is 9 meV, which is independent of temperature from the analysis of lowest temperature at 4.2 K PL spectra. It can be clearly seen that the homogeneous linewidths for the exciton peaks broadens linearly with increasing temperature. Moreover, the homogeneous broadening coefficients for the three different monolayer flakes (two flakes on SiO₂/Si and third on SiO₂) are nearly coincident, suggesting that the obtained values for the broadening coefficient reflect the intrinsic properties of monolayer MoTe₂. Homogeneous linewidths are generally determined by exciton dephasing, which is mainly caused by exciton–phonon scattering, and the radiative and non-radiative decay of excitons. Assuming a typical reported exciton relaxation time for TMDs greater than several picoseconds²³, the contribution to the linewidth from the exciton lifetime $\ll 1\text{meV}$ is expected to be negligible. Thus, the homogeneous linewidth broadening Γ is attributed to exciton–phonon scattering and described as follows:¹²

$$\Gamma = \Gamma_0 + AT + \frac{B}{\exp(\hbar\omega/k_B T) - 1}, \quad (2)$$

where Γ_0 is the residual linewidth at $T = 0$ K, A and B are exciton–phonon coupling constants for the low- and high-frequency phonon modes, respectively, $\hbar\omega$ is the energy of the high-frequency phonon mode, and k_B is Boltzmann’s constant. The solid lines in Fig. 5 show the fitted results obtained using eq. (2), and it can be clearly seen that they are in good agreement with the homogeneous linewidth broadening observed experimentally. The temperature dependence of the homogeneous linewidth exhibits nearly linear behavior over the wide temperature range from 4.2 to 300 K,

suggesting that the contributions of the high-frequency optical phonons are negligible and that exciton scattering with low-frequency acoustic phonons is the main cause of the homogeneous broadening of the exciton peak in the PL spectra for monolayer MoTe₂.

The value of the exciton–phonon coupling constant A was determined to be 0.11 meV/K for monolayer MoTe₂ on an SiO₂/Si substrate. Note that the same value was also obtained for monolayer MoTe₂ on a quartz substrate (see the Supporting Information, Fig. S4.). This value of A (0.11 meV/K) reflects the strength of exciton–phonon coupling and is nearly on the same order as the reported values for III-V (GaAs/AlGaAs) and II-VI (CdSe/ZnSe) semiconductor quantum wells^{24,25}. The small values for A (0.11 meV/K) and $B \sim 0.06$ meV/K suggest that monolayer MoTe₂ exists in the relatively weak exciton–phonon coupling regime. The energy difference between exciton absorptions and PL peaks, namely the Stokes shift, is another measure of exciton–phonon coupling and can be used to confirm the strength of exciton–phonon interactions²⁶. Thus, we measured the differential reflectivity spectra for monolayer MoTe₂ on a transparent quartz substrate (see Supporting Information, Fig. S1) which are close approximation of the absorption spectra⁷. Note that the exciton peaks in the differential reflectivity and PL spectra appear at the same energies, indicating a very small Stokes shift of less than 1 meV (see Supporting Information, Fig. S2). The very small Stokes shift also suggests that the exciton–phonon interactions in monolayer MoTe₂ are in the weak coupling regime, which is favorable for applications that require longer exciton coherence times²⁷.

In summary, we studied the PL and differential reflectance spectra for mechanically exfoliated monolayer MoTe₂ from 4.2 to 300 K. The PL spectra for monolayer MoTe₂ showed two sharp exciton and charged exciton (trion) peaks at low temperature. The homogeneous linewidth of the exciton peak underwent linear linewidth broadening with increasing temperature. The linear behavior of this temperature-dependent homogeneous linewidth broadening was attributed to acoustic-phonon scattering of excitons, which resulted in shortening of the exciton dephasing time. The homogeneous broadening factor due to these exciton–acoustic-phonon interactions was determined to be 0.11 meV/K. This relatively small value for the exciton–phonon coupling coefficient and the lack of a Stokes shift suggest that the exciton–phonon interactions in monolayer MoTe₂ are in the weak-coupling regime. Consequently, monolayer MoTe₂ as an atomically-thin-layered TMD has significant potential for use in optoelectronic device applications.

ACKNOWLEDGMENTS

The authors acknowledge S. Konabe for his fruitful discussions. This work was supported by Grants-in-Aid for Scientific Research from MEXT Japan (Nos. 22740195, 25400324, 24681031, 23340085, and 25610074) and by PRESTO from JST.

REFERENCES

- ¹ B. Baugher, H. Churchill, Y. Yang, and P. Jarillo-Herrero, *Nat. Nanotech.* **9**, 262 (2014).
- ² Q. Wang, K. Kalantar-Zadeh, A. Kis, J. N. Coleman, and M. S. Strano, *Nat. Nanotech* **7**, 699 (2012).
- ³ K. Fai Mak, K. He, C. Lee, G. H. Lee, J. Hone, T. F. Heinz, and J. Shan, *Nat. Mat.* **12**, 207 (2013).
- ⁴ Y. Lin, X. Ling, L. Yu, S. Huang, A. L. Hsu, Y-H. Lee, J. Kong, M. S. Dresselhaus, and T. Palacios, *Nano Lett.* **14**, 5569 (2014).
- ⁵ G. Wang, L. Bouet, D. Lagarde, M. Vidal, A. Balocchi, T. Amand, X. Marie, and B. Urbaszek, *Phys. Rev. B* **90**, 075413 (2014).
- ⁶ N. Zibouche, P. Philippsen, A. Kuc, and T. Heine, *Phys. Rev. B* **90**, 125440 (2014).
- ⁷ C. Ruppert, O. B. Aslan, and T. F. Heinz, *Nano Lett.* **14**, 6231 (2014).
- ⁸ I. G. Lezama, A. Arora, A. Ubaldini, C. Barreteau, E. Giannini, M. Potemski, and A. F. Morpurgo, *Nano Lett.* **15**, 2336 (2015).
- ⁹ N. R. Pradhan, D. Rhodes, S. Feng, Y. Xin, S. Memaran, B-H. Moon, H. Terrones, M. Terrones, and L. Balicas, *Acs Nano* **8**, 5911 (2014).
- ¹⁰ H. Guo, T. Yang, M. Yamamoto, L. Zhou, R. Ishikawa, K. Ueno, K. Tsukagoshi, Z. Zhang, M. S. Dresselhaus, and R. Saito, *Phys. Rev. B* **91**, 205415 (2015).
- ¹¹ H. Zhao, S. Wachter, and H. Kalt, *Phys. Rev. B* **66**, 085337 (2002).
- ¹² D. Karaiskaj and A. Mascarenhas, *Phys. Rev. B* **75**, 115426 (2007).

- 13 A. V. Trifonov, S. N. Korotan, A. S. Kurdyubov, I. Y. Gerlovin, I. V. Ignatiev, Yu P. Efimov, S. A. Eliseev, V. V. Petrov, Yu K. Dolgikh, V. V. Ovsyankin, and A. V. Kavokin, *Phy. Rev. B* **91**, 115307 (2015).
- 14 M. Yamamoto, S. T. Wang, M. Ni, Y-F Lin, S-L. Li, S. Aikawa, W-B. Jian, K. Ueno, K. Wakabayashi, and K. Tsukagoshi, *Acs Nano* **8**, 3895 (2014).
- 15 C. Mai, A. Barrette, Y. Yu, Y. G. Semenov, K. W. Kim, L. Cao, and K. Gundogdu, *Nano Letters* **14**, 202 (2014).
- 16 S. Fathipour, N. Ma, W. S. Hwang, V. Protasenko, S. Vishwanath, H. G. Xing, H. Xu, D. Jena, J. Appenzeller, and A. Seabaugh, *Appl. Phys. Lett.* **105**, 192101 (2014).
- 17 T. J. Wieting, A. Grisel, and F. Levy, *Physica B & C* **99** (1-4), 337 (1980).
- 18 M. Z. Bellus, F. Ceballos, H-Y Chiu, and H. Zhao, *Acs Nano*. **9**, 6459 (2015).
- 19 J. Yang, T. Lu, Y. W. Myint, J. Pei, D. Macdonald, J-C. Zheng, and Y. Lu, *Acs Nano* **9**, 6603 (2015).
- 20 Y. Li, Z. Qi, M. Liu, Y. Wang, X. Cheng, G. Zhang and L. Sheng, *Nanoscale*, **6**, 15248 (2014).
- 21 N. M. Ravindra and V. K. Srivastava, *J. Phys. Chem. Soli.* **40**, 791 (1979).
- 22 L. Vina, S. Logothetidis, and M. Cardona, *Phys. Rev. B* **30**, 1979 (1984).
- 23 Q. Cui, F. Ceballos, N. Kumar, H. Zhao, *Acs Nano*. **8**, 2970 (2014).
- 24 J. Feldmann, G. Peter, E. O. Gobel, P. Dawson, K. Moore, C. Foxon, and R. J. Elliott, *Phys. Rev. Lett.* **59**, 2337 (1987).
- 25 D. S. Citrin, *Solid State Commun.* **84**, 281 (1992).
- 26 S. Koirala, M. Takahata, Y. Hazama, N. Naka, and K. Tanaka, *J. Lumi.* **155**, 65 (2014).
- 27 G. Moody, C. K. Dass, K. Hao, C.-H. Chen, L.-J. Li, A. Singh, K. Tran,

G. Clark, X. Xu, G. Bergäuser, E. Malic, A. Knorr, and X. Li, Nat. Comm.
6, 8315 (2015).

FIGURE CAPTIONS

Figure 1. Raman scattering spectra for mechanically exfoliated monolayer, bilayer, and trilayer, and bulk MoTe₂ flakes on SiO₂/Si substrates obtained at an excitation wavelength of 532 nm. Left inset: optical microscope images of monolayer and bilayer MoTe₂ on SiO₂/Si substrates. Right inset: frequency shift of the E_{2g}¹ mode as a function of layer thickness.

Figure 2. Temperature dependence of the PL spectra for monolayer MoTe₂ and fitted results obtained using Voigt functions. The PL spectra are normalized by the intensity of the exciton peak. Each spectrum is vertically shifted for clarity.

Figure 3. PL spectra and fitted results for monolayer MoTe₂. (a) Upper panel: PL spectrum (blue line) and spectral fitted result obtained using the sum of Voigt functions (red line) at 4.2 K. Lower panel: Each component of the spectral peak. (b) Upper panel: PL spectrum (blue line) and spectral fitted result using the sum of Voigt functions (red line) at room temperature. Lower panel: Each component of the spectral peak.

Figure 4. Temperature dependence of the exciton (red solid squares) and trion (blue solid circles) peak positions in PL spectra for monolayer MoTe₂ and fitted lines obtained using the Varshni equation [eq. (1)].

Figure 5. FWHM of the exciton peak linewidth in PL spectra for monolayer MoTe₂ plotted as a function of temperature. The solid lines represent the fitted results obtained using eq. (2). The experimental results for three different monolayer MoTe₂ flakes on SiO₂/Si and SiO₂ are shown in the figure.

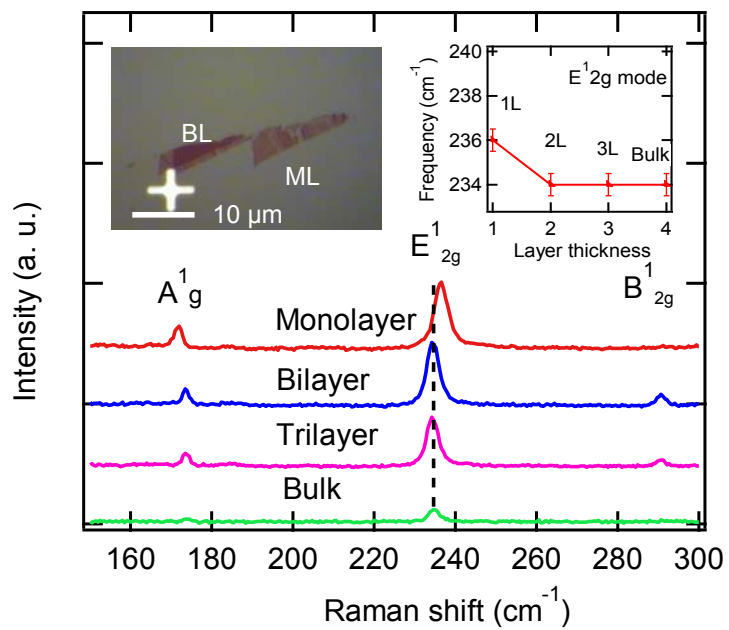


Fig. 1 S. Koirala et al.,

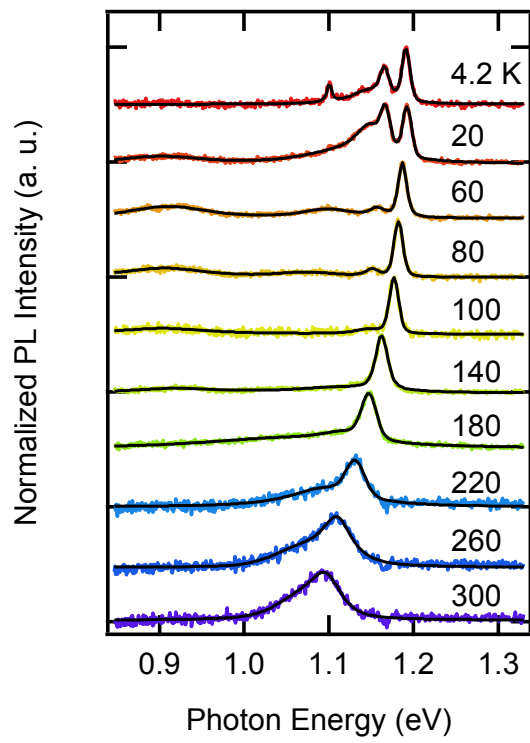


Fig. 2 S. Koirala et al.,

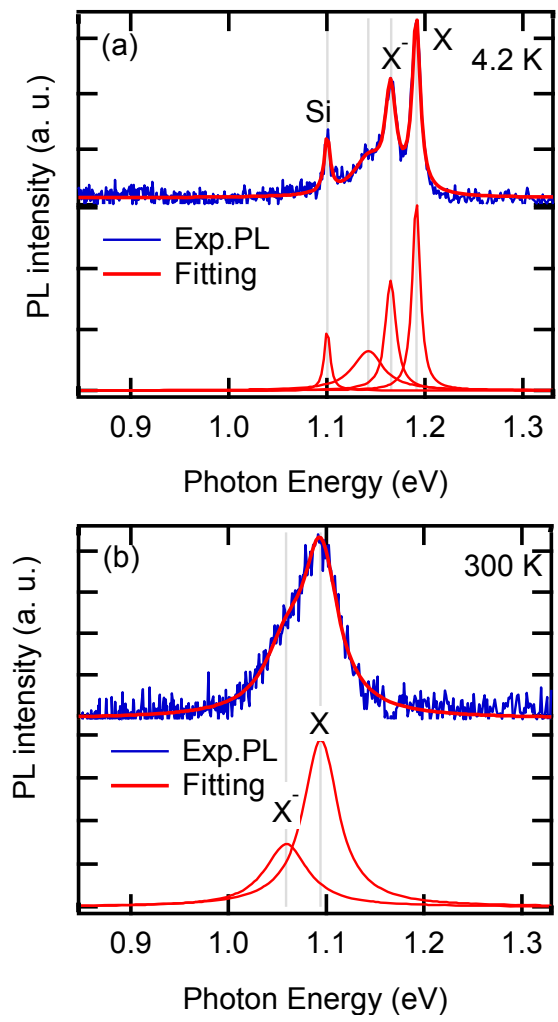


Fig. 3 S. Koirala et al.,

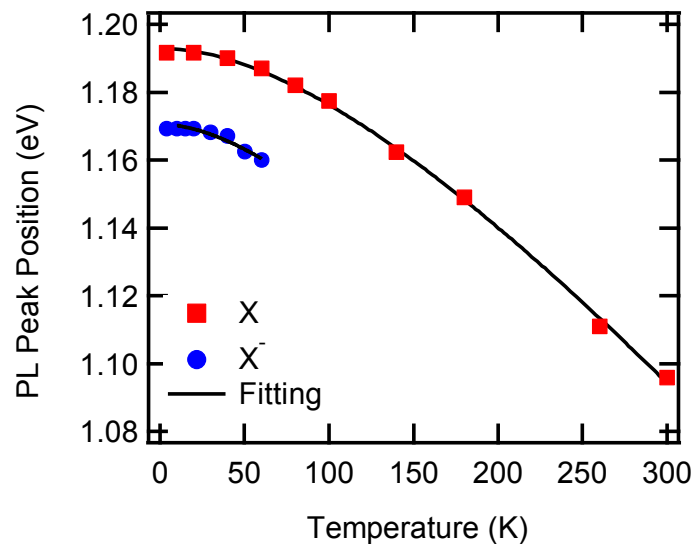


Fig. 4 S. Koirala et al.,

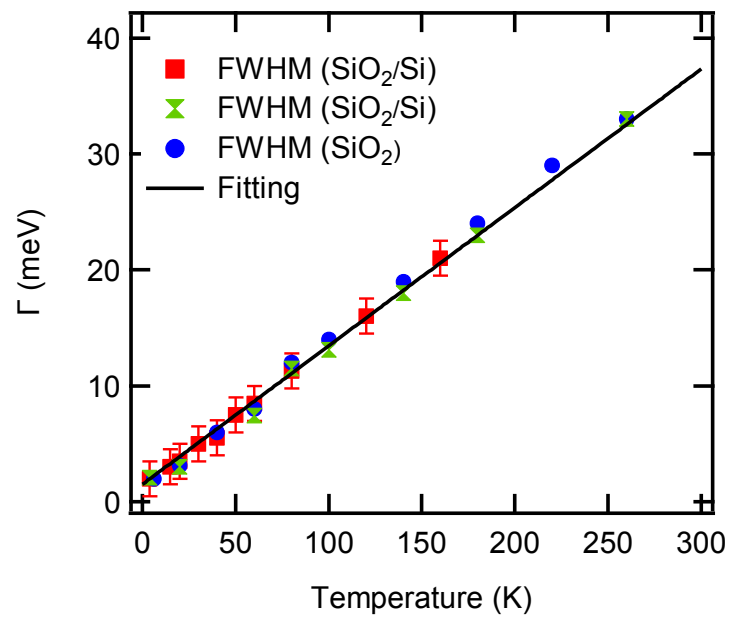


Fig. 5 S. Koirala et al .,